EXPLORING THE IMPACT OF OSMOADAPTATION ON GLYCOLYSIS USING TIME-VARYING RESPONSE-COEFFICIENTS

CLEMENS KÜHN[1] kuehn@molgen.mpg.de
ELZBIETA PETELENZ[2] elzbieta.petelenz@cmb.gu.se
BODIL NORDLANDER[2] bodil.nordlander@cmb.gu.se
JÖRG SCHABER[1] schaber@molgen.mpg.de
STEFAN HOHMANN[2] stefan.hohmann@gu.se
EDDA KLIPP[1] klipp@molgen.mpg.de

[1] *Computational Systems Biology Group, Max Planck Institute for Molecular Genetics, Ihnestraße 63-73, 14195 Berlin, Germany*
[2] *Department of Cell and Molecular Biology/Microbiology, University of Gothenburg Box 462 SE-405 30 Goeteborg, Sweden*

We present a model of osmoadaptation in *S.cerevisiae* based on existing experimental and theoretical work. In order to investigate the impact of osmoadaptation on glycolysis, this model focuses on the interactions between glycolysis and osmoadaptation, namely the production of glycerol and its influence on flux towards pyruvate. Evaluation of this model shows that, depending on initial relations between glycerol and pyruvate production, the increased glycerol production can have a substantial negative effect on the pyruvate production rate. Existing experimental data and a detailed analysis of the model lead to the suggestion of an interaction between activated Hog1 and activators of glycolysis such as Pfk26.

Keywords: osmoadaptation; yeast; Hog1; Pfk26; metabolic control analysis

1. Introduction

The yeast *Saccharomyces cerevisiae* is a unicellular eukaryote, frequently used as a model organism in biological research. Due to its relative simplicity and ease of cultivation *S. cerevisiae* is a convenient system to study a wide range of physiological and biochemical features conserved among eukaryotes, for example signal transduction via MAP kinase pathways [22]. One of the processes controlled by MAPK signaling in yeast is osmoregulation, mediated by the HOG (High Osmolarity Glycerol)[a] pathway. This pathway is activated in response to increased external osmolarity; it allows the cell to control its water and glycerol content, as well as

[a] Abbreviated molecule names mentioned in the text: DHAP: Dihydroxyacetone phosphate, F16BP: fructose-1,6-bisphosphate, F26BP: Fructose-2,6-bisphosphate F6P: fructose-6-phosphate, Fbp26: Fructose-2,6-bisphosphatase Fps1: glycerol channel, G3P: Glycerol 3-phosphate, GAP: Glyceraldehyde 3-phosphate Gpd1/2: NAD-dependent glycerol-3-phosphate dehydrogenase, Gpp1/2: DL-glycerol-3-phosphatase, Hog1: high osmolarity glycerol protein, Hog1PP: phosphorylated (active) form of Hog1, Pfk26: 6-phosphofructo-2-kinase, PFK: phosphofructokinase

other associated parameters like turgor pressure and cell volume [7]. The mechanisms governing adaptation after hyperosmotic shock in *S. cerevisiae* were elucidated by a substantial amount of existing experimental data as well as theoretical analyses [6, 11, 14]. During hyperosmotic shock, the extracellular osmotic pressure increases rapidly, causing the cell to lose water and thus volume, which is regained during osmoadaptation. As mentioned above, the mechanisms underlying osmoadaptation include activation of the HOG signalling pathway, the closure of the Fps1 glycerol channel and increased production of Gpd1, an enzyme crucial for glycerol production. The resulting increase in glycerol concentration raises the intracellular osmotic pressure, counterbalancing the increase in external osmotic pressure. Water - and volume - are regained. Since glycerol is a byproduct of glycolysis, we consider here the interactions and effects that glycolysis might have on osmoadaptation and vice versa.

For our theoretical analysis, we construct a model of ordinary differential equations (ODEs) based on previous models concerning adaptation to hyperosmotic stress [11] and modeling of glycolysis in yeast [9, 18, 20]. We analyze our resulting model using an extension of metabolic control analysis (MCA) that enables computation of sensitivities of species concentrations to parameter variations in a time-dependent manner, namely time-varying response coefficients (RCs) [10]. We use these time-varying RCs to characterize which reactions have major contributions to glycerol and pyruvate production in a time-dependent manner during osmoadaptation.

Simulation results of the model predict that osmoadaptation, with its increased production of glycerol, can significantly reduce pyruvate production (used here as a proxy for ATP production). Although this observation seems straightforward from the topology of the model given in Fig. 1, there is no experimental data available suggesting ATP depletion as a side effect of osmoadaptation. Ölz et al. [15] show that *S.cerevisiae* grown under saline conditions requires considerably more energy than grown on basal medium. Assuming, therefore, that pyruvate production might be maintained during osmoadaptation leads us to investigate possibilities to counteract this reduction in pyruvate production. The time-varying RCs show that the reaction F6P $\rightarrow$ F16BP is one of the most effective reactions in controlling pyruvate concentration and experimental results show that it is indeed associated with a protein known to be regulated by Hog1, namely Pfk26 [4, 5]. Incorporation of this interaction into the model results in a stabilized pyruvate concentration and an accelerated adaptation to hyperosmotic shock.

2. Methods

2.1. *Details of the model*

The model presented here is a simplification of the model presented in Klipp et al. [11] with additional modifications to the glycolysis module according to existing models of glycolysis. See Fig. 1 for an overview of the model topology. A list of

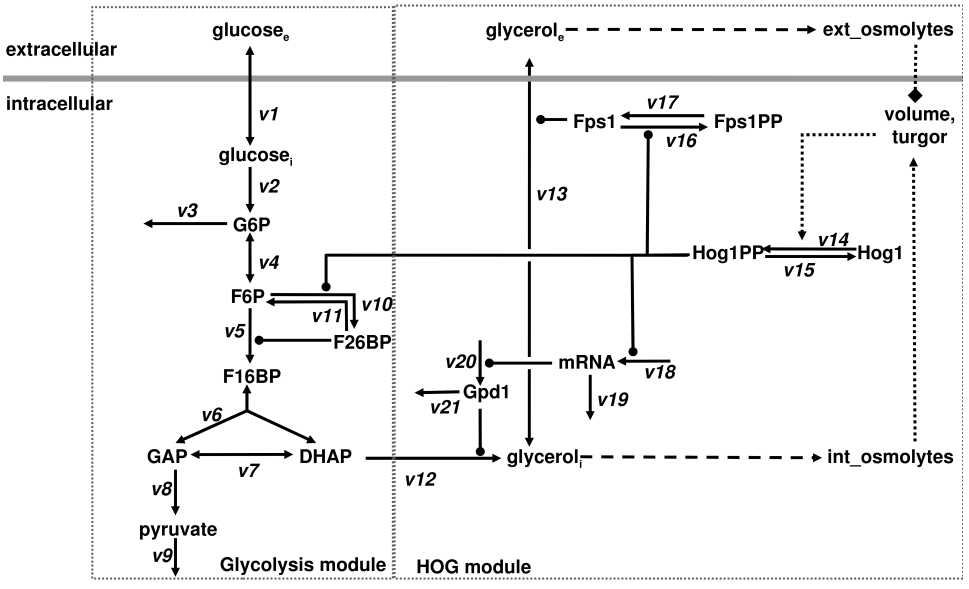

Fig. 1. Topology of the model described. Solid arrows indicate reactions, solid lines ending in filled circles indicate activation. Densely dashed arrows show positive influences, densely dashed lines ending in diamonds indicate negative inputs to a variable. Volume and turgor are combined because they are tightly interconnected. The loosely dashed arrows indicate that glycerol contributes to the intra- or extracellular osmolytes. The two modules of the model as described in the text are indicated by dashed rectangles. The exact allocation of a reaction to either of the modules might be ambiguous. Reaction v_{12}, for example, is part of both modules during parameter estimation.

all differential equations, initial conditions and parameter values can be found in supplementary data.

Here, we describe the major changes in relation to the previous model of osmoadaptation on yeast. The phosphorelay module as well as the MAPK module have been removed. Instead, Hog1 is transformed to Hog1-PP depending on $s(t)$, where

$$\frac{\mathrm{d}s(t)}{\mathrm{d}t} = k_s \cdot (1 - \frac{p(t)^{h_s}}{t_s^{h_s} + p(t)^{h_s}}) - k_s \cdot s(t) \tag{1}$$

with turgor pressure $p(t)$, k_s controlling the velocity of changes in $s(t)$, the value t_s, indicating the value of p at which the Hill-function is at half its maximal value and the Hill coefficient h_s. Activation and inactivation of Hog1 follows simple mass action kinetics. This significantly reduces model complexity while the extent of Hog1 activation still resembles experimental data (Fig. 3).

The computation of the turgor pressure has been modified according to Schaber

and Klipp [19]:

$$p(t) = \begin{cases} -\varepsilon * ln\frac{V(t)}{V_{p=0}} & \text{if } V(t) > V_{p=0} \\ 0 & else \end{cases} \tag{2}$$

with cell volume $V(t)$, ε as a measure of membrane elasticity and $V_{p=0}$ the volume at which turgor pressure becomes zero.

Modeling the nucleus as an individual compartment was omitted for reasons of simplicity. Transcription and translation are here considered only for *GPD1*. As only relative experimental data on Hog1 activity exist, we chose to set the initial concentration of inactive Hog1 to 1 and adjust the parameter values of the model accordingly.

Fps1 is not explicitly modeled as concentrations of an open and closed form but as the relative amount of open Fps1 channels as a measure of conductivity, an expression again based on the Hill-equation:

$$\frac{\mathrm{d}Fps1_o(t)}{\mathrm{d}t} = k_{v16} * p(t)^{h_{v16}}/(t_{v16}^{h_{v16}} + p(t)^{h_{v16}}) - k_{v17} * Fps1_o(t) \tag{3}$$

We furthermore reduced the two reactions DHAP $\leftrightarrow$ G3P $\rightarrow$ Glycerol, catalyzed by Gpd1/2 and Gpp1/2, respectively, to one reaction DHAP $\rightarrow$ Glycerol described with simple mass action kinetics. Although Cronwright et al [3] describe the regulation of Gpd1 in detail, we chose to simplify the regulation of Gpd1 here since most regulators are kept constant in this model.

To refine the glycolysis module of [11], we examined the individual rate laws for all reactions in three published models of yeast glycolysis [9, 18, 20] and checked each rate law for the underlying reasoning and its applicability here. For an overview over the individual rate laws please refer to the additional material.

In order to refine the model, we also consider an additional metabolite, F26BP, a glycolytic intermediate produced by the reaction F6P $\rightarrow$ F26BP (v_{10} here) catalyzed by Pfk26 [12] and degraded again by the reaction F26BP $\rightarrow$ F6P (v_{11}) catalyzed by Fbp26 [16]. F26BP is an activator of PFK (catalyzing v_5) and Pfk26 is reportedly activated by Hog1PP [5]. The activation by Hog1PP is incorporated following a Michaelis-Menten kinetic for F6P $\rightarrow$ F26BP modified to include two different Km-Values, one for the Hog1PP-activated form of Pfk26 and one for the basal activity:

$$v10(t) = \frac{k_{v10vmax} \cdot F6P(t)}{F6P(t) + \frac{Hog1PP(t)}{Hog1PP(t)+k_{v10k}} \cdot k_{v10Km2} + \frac{k_{v10k}}{Hog1PP(t)+k_{v10k}} \cdot k_{v10Km1}} \tag{4}$$

where the activity of Pfk26 is indicated by the fraction $\frac{Hog1pp(t)}{Hog1pp(t)+k_1}$. This fraction is multiplied by k_{v10Km2}, a lower Km-value than k_{v10Km1} corresponding to the inactive form. The backwards reaction, catalyzed by Fbp26 is modeled using simple mass action kinetics. Because the concentration of F26BP is very low (0.00014mM before stress, 0.0002mM after activation by Hog1PP) compared to the concentrations of both F6P (0.165mM initially) and F16BP (0.425mM initially), activation

of F26BP production does not decrease F16BP formation by redirection of reaction flux.

In contrast to the underlying models, this model does not contain dynamic concentrations of ADP, ATP, AMP, NAD and NADH for simplicity.

The SBML model was created and modified using Copasi [8] in version 4.4, build 25, which enables the integration of volume changes in the formulation of the SBML model.

2.2. *Experimental data and parameter estimation*

The experimental data used to fit the parameters have mostly been obtained from [11] for the part of osmoadaptation. Experimental data on glycolysis have been extrapolated from the models noted before [9, 18, 20]. Due to the large number of different yeast strains combined with the vast number of possible experimental settings (e.g. choice of medium and aerobicity), the differences in metabolite concentrations between experiments can be immense. We take the set of metabolite concentrations mainly from [18]. Although these concentrations were also obtained from anaerobic experiments, the cytosolic free NAD and NADH concentrations agree better with recent measurements [2] than the measurements from [9, 20]. Please refer to Supplementary Table 1 for the choice of the values and a comparison to other experimental data.

After sensible initial metabolite concentrations were set, the reaction parameters of both the glycolysis module (for parameter estimation, this module contains reactions v_1 to v_{12} and a glycerol degrading reaction following mass action kinetics) and the HOG module (including reactions v_{12} to v_{21} and the dynamics of volume and turgor pressure in this context) had to be modified in order to create a steady state of the system before application of the stress and reproduce the experimental data on osmoadaptation. As Teusink et. al. [20] have pointed out, enzyme properties measured in vitro are not necessarily directly applicable to mathematical models. In order to find a set of parameters that generates the desired concentrations, we resorted to parameter estimation although the experimental data is too sparse to allow for the identification of a unique set of parameters satisfying the experimental data.

When estimating a large number of parameters for a system, it might considerably speed up the computation process to divide the model into subsystems that can be joined after a lightweight parameter estimation task for each of the subsystems has been applied [13]. We accordingly divided the model into the glycolysis and HOG module that could be joined after the parameters were fitted. The glycolysis module does not contain a variable cell volume and could be fitted using SBML-PET [23]. The parameters of the HOG module were fitted by hand using the results of previous models.

2.3. *Computation of time-varying response coefficients*

Response coefficients (RCs) are a standard measure of MCA, indicating the sensitivity of steady state concentrations to infinitesimally small changes in some parameter. In order to capture the sensitivities during the course of osmoadaptation, we employ an extension of this notion proposed by Ingalls and Sauro [10]. Scaled time-varying response coefficient $R_q^s(t)$ are defined as

$$R_q^s(t) = \frac{q}{s} \cdot \frac{\partial s(t,q)}{\partial q}|_{q=q_0} \tag{5}$$

and is a measure for the sensitivities of substance concentrations s to an infinitesimally small variation in the set of initial conditions s_0 and parameters p_0 where $q_0 = s_0 \cup p_0$. The concentration of the species s is a function of time t and q, $s(t,q)$.

These time-varying response coefficients are scaled by the scaling factor $\frac{q}{s}$ and are computed together with the computation of the trajectory. Scaled time-varying RCs have been computed for all parameters in the reaction network, using Wolfram Mathematica version 6.0.2 [17].

3. Results and Discussion

3.1. *Simulation of model*

The model including Pfk26 qualitatively reproduces known experimental data on the adaptation to hyperosmotic shock. Fig. 3 shows the key components of osmoadaptation after a hyperosmotic shock with 0.5M NaCl. The conductivity of the glycerol channel Fps1 is rapidly reduced upon shock, Hog1 is phosphorylated to its active form and triggers transcription of *GPD1* mRNA. Hog1-phosphorylation has a peak at 250 seconds (4.2 minutes) after the application of the shock and then declines again. The concentration of *GPD1* mRNA transiently rises to a peak at about 1800 seconds (30 minutes) after shock while the Gpd1 concentration reaches its maximal concentration more than 3000 seconds (50 minutes) after the shock. The glycerol concentration has a sharp initial rise due to decrease of volume and closure of Fps1 followed by an increase due to Gpd1-dependent production and saturates at about 2500 seconds (42 minutes) after the shock. The cell volume (not shown) rapidly decreases to about 70% of its initial value, after which it increases again as the intracellular glycerol concentration increases.

Our model does not lead to perfect adaptation, but perfect adaptation can be achieved with the described model using different parameter settings. The reason we do not use perfect adaptation in this model is that existing experimental data do not produce a clear and unambiguous answer to the question whether perfect adaptation is achieved for this amount of stress.

The metabolites involved in glycolysis remain in steady state without addition of osmotic shock. After application of the shock and adaptation, the system switches to a new steady state, as given in Supplementary Table 1. For a model without

activation of Pfk26 (*NoPfk26*), this evaluation of metabolic intermediates reveals a decrease in many metabolite concentrations following the osmotic shock, which is a result of the increased drain by increased glycerol production. The severity of this effect crucially depends on the initial balance of glycerol production and pyruvate production, $\frac{v_8}{v_{12}}$. A comparison between osmoadaptation of three different models is given in Fig.2 and Supplementary Table 1. Depicted in the figure are three different models, *NoPfk26*, *Glycerol* and *Pfk26*. Model *Glycerol* is derived from *NoPfk26*, but the parameters of the glycolysis module have been changed to increase v_{12} by a factor of 10 without changing the metabolite concentrations. Model *Pfk26* is the model including activation of Pfk26, as described in section 2 and depicted in Figures 1,3,4,6,5. While model *Pfk26* results in an increase in glycerol and pyruvate after osmotic shock, the glycerol concentration in model *NoPfk26* rises slower and the pyruvate concentration decreases. In model *Glycerol*, the chosen reaction parameters do not allow for a sufficient increase in glycerol concentration and thus the volume cannot be regained. The increased flux towards glycerol leads to a strong decrease in pyruvate production and both concentrations eventually level out.

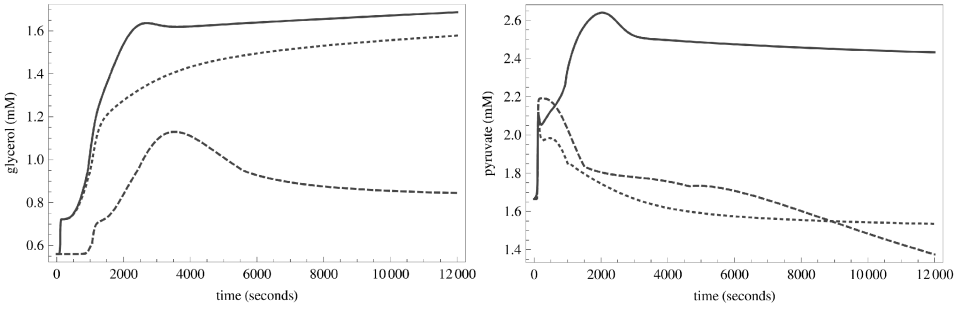

Fig. 2. Simulation results for glycerol (left) and pyruvate (right) concentrations during osmoadaptation using different models. The solid line refers to model *Pfk26*, the thick dotted line refers to model *NoPfk26* and the thin dotted line refers to model *Glycerol*. The different models are discussed in the text, stress is applied at $t = 100$.

A decrease in metabolite concentrations during osmoadaptation has not yet been detected in experimental data. Although it is arguable that pyruvate and other metabolite concentrations need to be constant during adaptation to osmotic shock, the experimental data underlying the activation of Pfk26 suggested its incorporation into the model. This mechanism is also indicated by the drastic effects of a low $\frac{v_8}{v_{12}}$ as shown in Fig 2.

In order to support the incorporation of Pfk26, we resorted to the time-varying RCs as described later to detect alterations in the reaction network to which the pyruvate concentration is highly sensitive. Together with v_2 and v_4, v_5 could be identified as a susceptible target for regulation in order to increase glycolytic flux because parameters of these reactions have the greatest RCs on pyruvate concentration during osmotic shock. The activation of Pfk26 as described in [5] would increase

flux through reaction v_5 because Pfk26 is one of two isoenzymes that catalyze the reaction F6P $\rightarrow$ F26BP [1] (here v_{10}). The role of F26BP has been discussed in Methods, as well as the kinetics used to incorporate F26BP into the model. As F26BP is an activator of PFK, an increase in F26BP can increase glycolytic flux upstream of the branch dividing pyruvate and glycerol production, thus increasing flux to both reactions.

Simulations of the model *Pfk26* including activation of Pfk26 result in a different steady state after adaptation to osmotic shock than simulations without this activation, as given in Supplementary Table 1 and Fig. 2, showing significantly increased instead of reduced metabolite concentrations. Furthermore, in the model including F26BP, the time osmoadaptation takes is reduced and glycerol production increased. Although the initial intention was to stabilize the pyruvate concentration, we momentarily accept the resulting increase in pyruvate concentration until new experimental data becomes available.

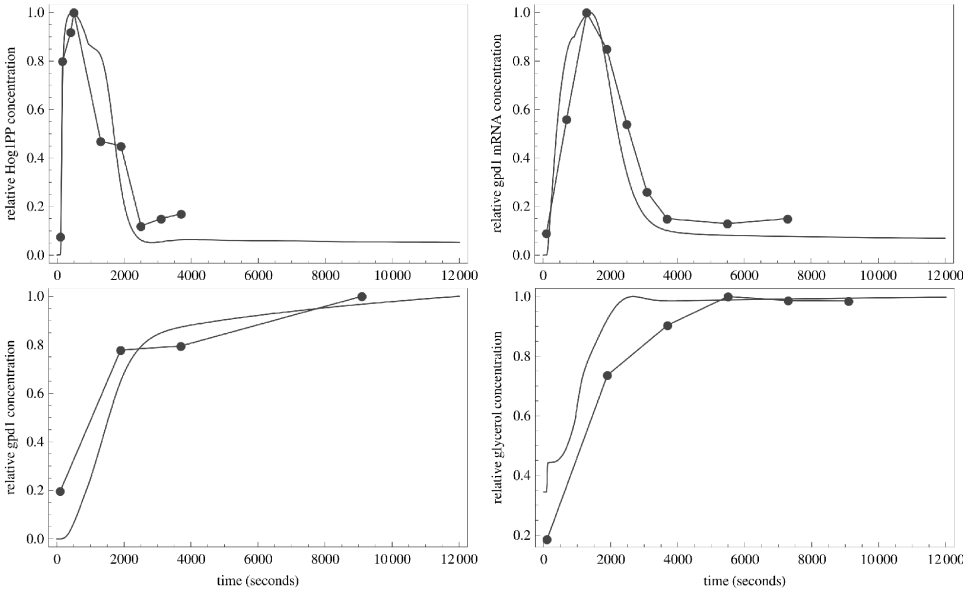

Fig. 3. Experimental data and simulation results for the model without Pfk26 activation. Lines with points show experimental data, smooth lines show simulation results. Clockwise, from top left: Hog1PP, *GPD1* mRNA, glycerol, Gpd1. Experimental data from [11].

3.2. *Time-varying response coefficients*

In the following, we present selected time-varying response coefficients for pyruvate and glycerol for the system with integrated Pfk26-activation. Positive values of $R(t)_y^x$ indicate that parameter y has a positive effect on concentration x at time point t, an increase in y would increase x. Negative values of $R(t)_y^x$ indicate that an

increase in y would lead to a decrease in x at time point t. Using time-varying RCs, we are able to discriminate between temporary effects, where $R(t)_y^x$ deviates from 0 for a very short time and long-lasting effects, where $R(t)_y^x$ is significantly positive or negative for a longer period of time. Below we discuss and interpret the values of the individual RCs.

The $R(t)_q^{glycerol}$ and $R(t)_q^V$ are similar. Generally, we observe for both glycerol and pyruvate that the RCs for parameters involved in the HOG module (containing reactions v_{14} to v_{21}) are smaller than for parameters involved in the glycolysis module (reactions v_1 to v_{13}) by about one order of magnitude. This is due to the fact that glycolytic parameters control the net glycolytic flux, and thus the concentration of metabolites even in the absence of HOG signalling. The response coefficient for the parameters pertaining to $Vmax$ in Michaelis-Menten kinetics are the largest except for the reversible v_4, for which the equilibrium constant is maximal.

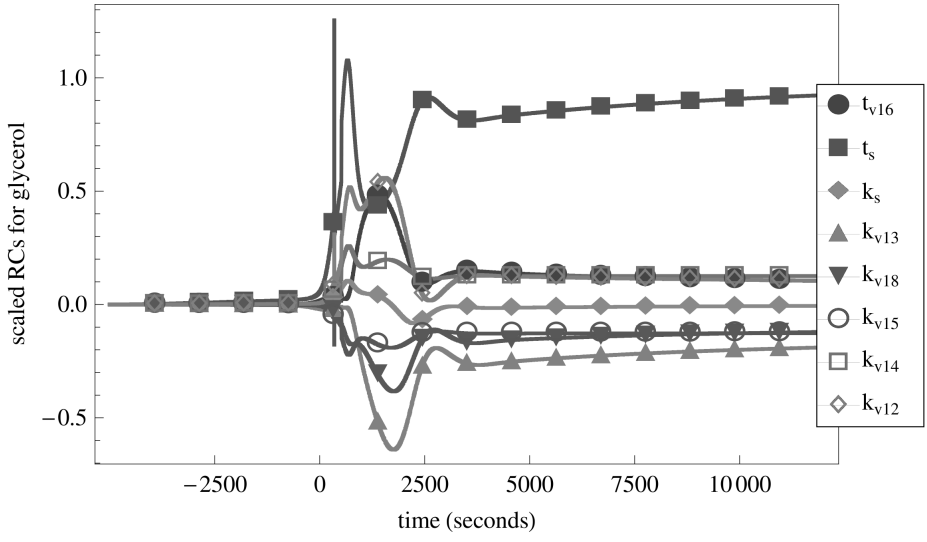

Fig. 4. RCs for glycerol concentration for selected parameters of the HOG module. Osmotic stress is applied at $t = 0$. Markers for each curve are inserted for distinction at arbitrary intervals. t_{v16} and t_s are the parameters giving the thresholds of turgor change that cause Fps1 and Hog1 changes. k_s determines the speed of Hog1 activation, k_{v13} the rate of glycerol transport, k_{v19} the rate for mRNA degradation, k_{v14} and k_{v15} are the rate constants for Hog1 phosphorylation/dephosphorylation and k_{v12} is the rate constant used in glycerol production. For detailed kinetics see the model in supplementary data.

The RCs for glycerol concentration and HOG module parameters, $R(t)_{HOG}^{glycerol}$ are distinguishable into early and late parameters, as can be seen in Fig. 4. k_{v14} (determining the speed of Hog1 activation) and k_{v15} (determining the speed of Hog1PP inactivation), have stronger impact before 1000 seconds (16.6 minutes) after shock. Once the maximal activation is achieved, small changes in these parameters have

no great impact anymore. While t_{v16}, the threshold parameter in Fps1 closure, k_{v12} (involved in glycerol production) and k_{v13} (involved in glycerol transport) both have greater impact later than 1000 seconds after the onset of stress. t_s, the threshold parameter controlling activation of Hog1, has a high impact before 1000 seconds after shock, the $R(t)_{ts}^{glycerol}$ then declines again but rises almost to its previous maximum again 2500 seconds (41.6 minutes) after shock. This delayed impact of the threshold parameters is connected with the magnitude of the volume change, since the associated turgor pressure initially declines very rapidly past the threshold parameters. But as the volume is regained, turgor pressure approaches the threshold parameters again, therefore increasing their impact on the system.

As for parameters of the HOG module, parameters involved in glycolysis have virtually no influence on glycerol concentration before the onset of shock. After application of the osmotic shock, all $R(t)_{glycolysis}^{glycerol}$ have transient increases during the phase of Hog1 activity and volume regulation, but once the cell volume is stabilized, the $R(t)_{glycolysis}^{glycerol}$ decline again. The parameters involved in v_2, v_3 and v_4 exhibit the highest RCs during osmoadaptation.

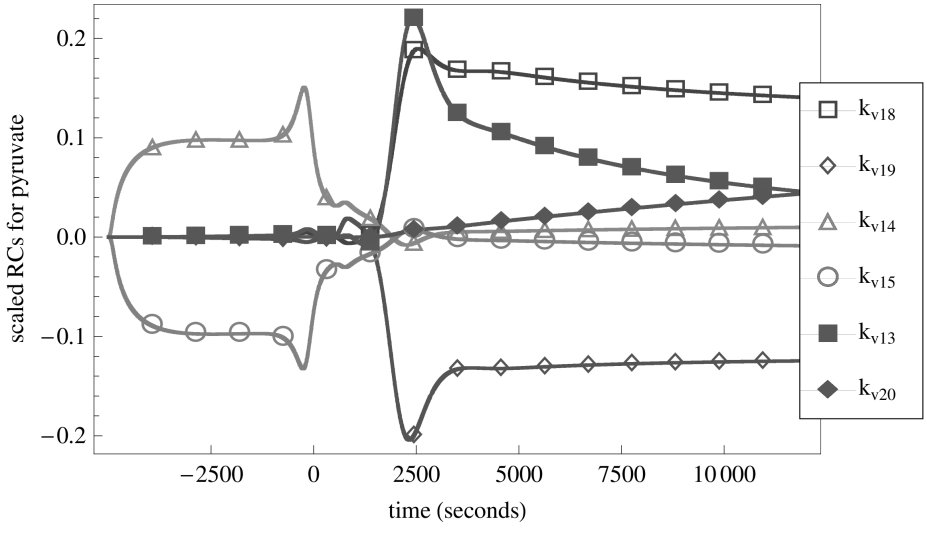

Fig. 5. RCs of pyruvate concentration for selected parameters of the HOG module. Osmotic stress is applied at $t = 0$. k_{v19} determines the rate of mRNA degradation, k_{v20} that of Gpd1 translation, k_{v14} and k_{v15} determine the speed of Hog1 phosphorylation and dephosphorylation, respectively. k_{v13} is involved in glycerol transport and k_{v21} is the rate constant for Gpd1 degradation. Detailed kinetics can be found in the model in supplementary data. Markers for each curve are inserted for distinction at arbitrary intervals.

The $R(t)_{HOG}^{pyruvate}$ before the onset of the shock show a high positive value for $R(t)_{k_{v14}}^{pyruvate}$ and a high negative value for $R(t)_{k_{v15}}^{pyruvate}$, due to the increase in glycolytic flux through Hog1-dependent Pfk26 activation. This activation of Pfk26

seems to outperform the Hog1-dependent increase in Gpd1 concentration for low levels of activation. After stress is applied, these Hog1-regulating RCs vanish and $R(t)^{pyruvate}_{k_{v20}}$, $R(t)^{pyruvate}_{k_{v18}}$ and $R(t)^{pyruvate}_{k_{v19}}$ (all three regarding production/degradation of Gpd1 or *GPD1* mRNA) as well as $R(t)^{pyruvate}_{k_{v13}}$ (glycerol transport) rise sharply. During the course of osmoadaptation, $R(t)^{pyruvate}_{k_{v21}}$ slowly increases as $R(t)^{pyruvate}_{k_{v13}}$. This is caused by the redirection of glycolytic flux to glycerol production caused by high levels of Gpd1. This behavior is depicted in Fig.5.

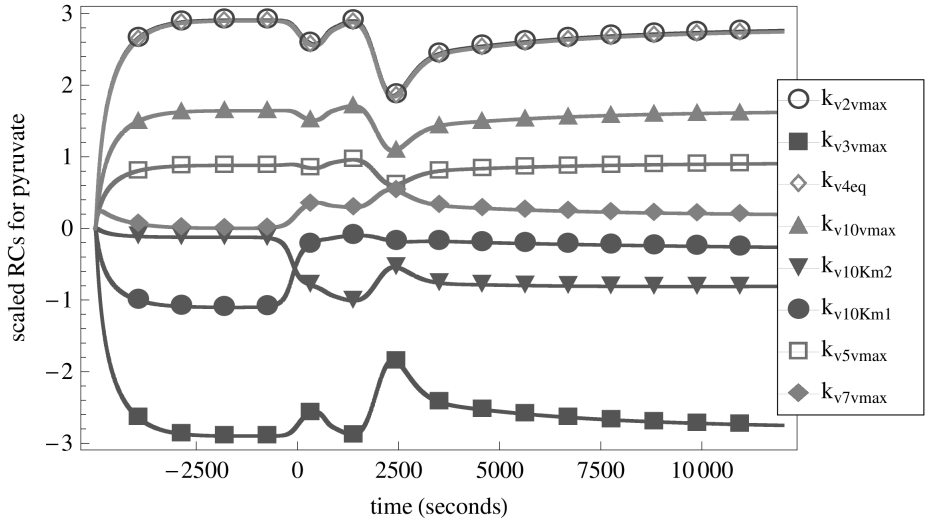

Fig. 6. RCs of pyruvate concentration for selected parameters of glycolysis, osmotic stress applied at $t = 0$. Markers for each curve are inserted for distinction at arbitrary intervals. The parameters shown are the most relevant parameters of the reactions with the associated number in Fig. 1. k_{v10Km1} and k_{v10Km2} are the two different Km-values used in the activation of Pfk26. k_{v4eq}, the equilibrium constant of v_4 was chosen here since it generally has a greater time-varying RC than k_{v4vmax}, the corresponding rate constant. Detailed kinetics of each reaction are given in the model in supplementary data.

The strongest $R(t)^{pyruvate}_{glycolysis}$ are shown in Fig. 6. Since alterations in these parameters change glycolytic flux even in the absence of HOG-signaling, the pyruvate concentration is always sensitive to these parameters. The sensitivity of the pyruvate concentration to glycolytic parameters generally decreases during osmoadaptation but rises again after adaptation is achieved. One exception is $R(t)^{pyruvate}_{k_{v10vmax}}$, which increases glycolytic flux during osmoadaptation. This parameter indicates that the rate of v_{10} has the greatest impact on pyruvate concentration during osmoadaptation. The RCs for the two Km-values for the different states of Pfk26, $R(t)^{pyruvate}_{k_{v10Km1}}$ and $R(t)^{pyruvate}_{k_{v10Km2}}$, show a switch like behavior during osmoadaptation: Before the osmotic shock, $R(t)^{pyruvate}_{k_{v10Km1}}$ is greater, but as Pfk26 is activated by Hog1, $R(t)^{pyruvate}_{k_{v10Km2}}$ rises as the role of k_{v10Km1} decreases. This switch in impact of the two parameters

is not transient.

The detection of this switch-like behavior exemplifies the advantage of time-varying response coefficients compared to standard response coefficients. The changes in response coefficients observed in this analysis also suggest that there need not be one exclusive rate limiting reaction in a metabolic pathway but that this property is distributed over all reactions and the specific values might heavily depend on the state of cell.

4. Conclusion

We have revisited existing models of osmoadaptation in order to focus on the impact of individual parameters on glycerol production and on the balance between glycerol and pyruvate production. We incorporated new experimental evidence on Pfk26 and performed a systematic exploration of the model behavior. The refinement of the model resulted in the following predictions: Activation of Pfk26 by Hog1PP leads to a significantly increased glycolytic flux during osmoadaptation and a decelerated osmoadaptation in case of Pfk26 knockout. Although the exact extent of the increase in glycolytic flux needs to be determined experimentally, the model shows that activation of Pfk26 by Hog1PP has a crucial role in maintaining a stable pyruvate level or even increasing this level during osmoadapataion. This provides the cell with additional energy during adaptation and protects it from starvation. By increasing the glycolytic flux, Pfk26 also has substantial influence on the rate of osmoadaptation because it provides the reaction DHAP $\rightarrow$ G3P with an increased substrate concentration. The importance of this effect might vary under different conditions: If the initial glycolytic flux is high, maintenance of the pyruvate concentration might be more crucial than an increase in glycerol production due to increased glycolytic flux. If the glycolytic flux is initially low, an increase in glycerol production besides the Gpd1-mediated increase might be favorable. Using this rather simple mechanism, the yeast cell gains both a boost in adaptation speed and energy supply under stress conditions.

The RCs for this system do not show one rate limiting reaction for glycolytic flux. Contrary to popular opinion, parameters of three reactions (v_2, v_3 and v_4) have equally large absolute values for their RC on pyruvate concentration, which indicates that all three have a similar effect on glycolytic flux. Furthermore, they decrease during the simulation and get close to the RC of even a fourth reaction. There are many of these transient changes in RCs during osmoadaptation. This indicates that the extent to which a reaction influences the net flux through a pathway can vary greatly depending on the external conditions and state of the cell. It might therefore be more sensible to speak of a rate limiting reaction or a group of rate limiting reactions under certain conditions.

Acknowledgments

Clemens Kühn is funded by the International Research Training Group 'Genomics and Systems Biology of Molecular Networks', supported by the German Research Foundation (DFG). Elzbieta Petelenz is a fellow in the EC-funded Marie Curie EST project 'Systems Biology' (514169). Jörg Schaber is supported by the European Commission (CELLCOMPUT (043310)). Work in the Hohmann Lab is supported by Vetenskapsrådet and in both the Hohmann and the Klipp labs by the European Commission (QUASI (030710) and UNICELLSYS (201142)).

References

[1] Bedri, A., Kretschmer, M., Schellenberger, W., and Hofmann, E., Kinetics of 6-phosphofructo-2-kinase from *Saccharomyces cerevisiae*: inhibition of the enzyme by ATP, *Biomedica Biochimica Acta*, 48(7):403–411, 1989.

[2] Canelas, A. B., van Gulik, W. M., and Heijnen, J. J., Determination of the cytosolic free nad/nadh ratio in *Saccharomyces cerevisiae* under steady-state and highly dynamic conditions, *Biotechnol Bioeng*, Jan 2008.

[3] Cronwright, G. R., Rohwer, J. M., and Prior, B. A., Metabolic control analysis of glycerol synthesis in *Saccharomyces cerevisiae*, *Appl Environ Microbiol*, 68(9):4448–4456, Sep 2002.

[4] Dihazi, H., Kessler, R., and Eschrich, K., Phosphorylation and inactivation of yeast 6-phosphofructo-2-kinase contribute to the regulation of glycolysis under hypotonic stress, *Biochemistry*, 40(48):14669–14678, Dec 2001.

[5] Dihazi, H., Kessler, R., and Eschrich, K., High osmolarity glycerol (hog) pathway-induced phosphorylation and activation of 6-phosphofructo-2-kinase are essential for glycerol accumulation and yeast cell proliferation under hyperosmotic stress, *J Biol Chem*, 279(23):23961–23968, Jun 2004.

[6] Gennemark, P., Nordlander, B., Hohmann, S., and Wedelin, D., A simple mathematical model of adaptation to high osmolarity in yeast, *In Silico Biol*, 6(3):193–214, 2006.

[7] Hohmann, S., Osmotic stress signaling and osmoadaptation in yeasts, *Microbiol Mol Biol Rev*, 66(2):300–372, Jun 2002.

[8] Hoops, S., Sahle, S., Gauges, R., Lee, C., Pahle, J., Simus, N., Singhal, M., Xu, L., Mendes, P., and Kummer, U., Copasi–a complex pathway simulator, *Bioinformatics*, 22(24):3067–3074, Dec 2006.

[9] Hynne, F., Danø, S., and Sørensen, P. G., Full-scale model of glycolysis in *Saccharomyces cerevisiae*, *Biophys Chem*, 94(1-2):121–163, Dec 2001.

[10] Ingalls, B. P. and Sauro, H. M., Sensitivity analysis of stoichiometric networks: an extension of metabolic control analysis to non-steady state trajectories, *J Theor Biol*, 222(1):23–36, May 2003.

[11] Klipp, E., Nordlander, B., Krüger, R., Gennemark, P., and Hohmann, S., Integrative model of the response of yeast to osmotic shock, *Nat Biotechnol*, 23(8):975–982, Aug 2005.

[12] Kretschmer, M. and Fraenkel, D. G., Yeast 6-phosphofructo-2-kinase: sequence and mutant, *Biochemistry*, 30(44):10663–10672, Nov 1991.

[13] Kühn, C., Kühn, A., Poustka, A. J., and Klipp, E., Modeling development: spikes of the sea urchin, *Genome Inform*, 18:75–84, 2007.

[14] Mettetal, J. T., Muzzey, D., Gómez-Uribe, C., and van Oudenaarden, A., The

frequency dependence of osmo-adaptation in *Saccharomyces cerevisiae*, *Science*, 319(5862):482–484, Jan 2008.

[15] Ölz, R., Larsson, K., Adler, L., and Gustafsson, L., Energy flux and osmoregulation of *Saccharomyces cerevisiae* grown in chemostats under NaCl stress, *J Bacteriol*, 175:2205–2213, Apr 1993.

[16] Paravicini, G. and Kretschmer, M., The yeast fbp26 gene codes for a fructose-2,6-bisphosphatase, *Biochemistry*, 31(31):7126–7133, Aug 1992.

[17] Research, W., *Mathematica, Version6.0*, Wolfram Research, Champaign, IL, 2007.

[18] Rizzi, M., Baltes, M., Theobald, U., and Reuss, M., In vivo analysis of metabolic dynamics in *Saccharomyces cerevisiae* ii. mathematical model, *Biotechnol Bioeng*, 55:592–608, 1997.

[19] Schaber, J. and Klipp, E., Short-term volume and turgor regulation in yeast, *Essays in Biochemisty*, 2008.

[20] Teusink, B., Passarge, J., Reijenga, C. A., Esgalhado, E., van der Weijden, C. C., Schepper, M., Walsh, M. C., Bakker, B. M., van Dam, K., Westerhoff, H. V., and Snoep, J. L., Can yeast glycolysis be understood in terms of in vitro kinetics of the constituent enzymes? Testing biochemistry, *Eur J Biochem*, 267(17):5313–5329, Sep 2000.

[21] Theobald, U., Mailinger, W., Baltes, M., Rizzi, M., and Reuss, M., In vivo analysis of metabolic dynamics in *Saccharomyces cerevisiae*: I. experimental observations, *Biotechnol Bioeng*, 55(2):305–316, July 1997.

[22] Widmann, C., Gibson, S., Jarpe, M. B., and Johnson, G. L., Mitogen-activated protein kinase: conservation of a three-kinase module from yeast to human, *Physiol Rev*, 79(1):143–180, Jan 1999.

[23] Zi, Z. and Klipp, E., SBML-PET: a systems biology markup language-based parameter estimation tool, *Bioinformatics*, 22(21):2704–2705, Nov 2006.